nature biotechnology

Article

https://doi.org/10.1038/s41587-025-02685-x

Efficient mitochondrial A-to-G base editors for the generation of mitochondrial disease models

Received: 23 January 2025

Accepted: 24 April 2025

Published online: 03 June 2025

Check for updates

Liang Chen[1,2,3,11] ✉, Mengjia Hong[1,11], Changming Luan[1,11], Meng Yuan[1], Yiming Wang[2], Xinyuan Guo[1], Yue Fang[4,5], Hao Huang[1], Xiaohua Dong[2,6], Hongyi Gao[1], Dan Zhang[1], Xi Chen[7], Dihao Meng[1], Molin Huang[1], Zongyi Yi[8], Mingyao Liu[1,7], Wensheng Wei[8,9], Liangcai Gao[1], Gaojie Song[1], Xiaoming Zhou[4,5] & Dali Li[1,3,10] ✉

Existing A-to-G base editors for mitochondrial DNA (mtDNA) are limited by low efficiency. We used directed evolution to discover variants of the TadA-8e base editors that have substantially increased activity and expanded targeting compatibility for both nuclear and mitochondrial adenine base editing, especially in previously unfavored sequence contexts. The engineered mtDNA editors (eTd-mtABEs) showed up to 87% editing efficiency in human cells, with greatly reduced DNA and RNA off-target effects. Strand-selective A-to-G editing was enhanced by an average of 3.2-fold with substitution of DddA to DNA nickases in eTd-mtABE backbones compared to mitochondrial ABEs. In rat cells, editing efficiencies of eTd-mtABEs were up to 145-fold higher compared to split DddA transcription activator-like effector-linked deaminase. We also generated rats with sensorineural hearing loss by installing targeted mutations with frequencies of up to 44% through embryonic injection. The developed eTd-mtABEs are efficient and precise mtDNA-engineering tools for basic research and translational studies.

Mutations in mitochondrial DNA (mtDNA) have been associated with genetic diseases including Leber hereditary optic neuropathy (LHON), mitochondrial encephalomyopathy with lactic acidosis and stroke-like episodes (MELAS) and Leigh syndrome, with an estimated prevalence of ~1 in 5,000 (refs. 1,2). Among 95 pathogenic mutations in mtDNA genes, 95% (90/95) of them are point mutations[1–3]. In contrast to research on genetic disorders caused by nuclear genes, genetic manipulation of mammalian mtDNA has been difficult, hampering mechanistic studies and the development of therapeutics for mtDNA diseases[4,5]. A method is available to create transmitochondrial cytoplasmic hybrid cells (cybrids), which permits the generation of cells and mouse models that mimic mitochondrial diseases[6]. However, its technical complexity, coupled with the scarcity of technologies to induce targeted mtDNA mutations, renders the development of mitochondrial disease models challenging[5,7].

mtDNA can be targeted through customized nucleases. A heteroplasmy shift toward wild-type mtDNA is achievable through site-specific nucleases, specifically mitochondrially targeted restriction endonucleases and programmable nucleases, including zinc-finger nucleases (ZFNs), transcriptional-activator-like effector (TALE) nucleases and ARCUS nucleases, in transmitochondrial cells or mouse models[5,8–11]. These encouraging studies shed light on the development of therapeutics for mtDNA diseases. However, because the programmable nucleases are unable to induce specific point mutations, which are the major type of pathogenic mtDNA mutations, targeted engineering of mtDNA to model human mitochondrial disorders

A full list of affiliations appears at the end of the paper. ✉e-mail: chenliang@lglab.ac.cn; dlli@bio.ecnu.edu.cn

https://doi.org/10.1038/s41587-025-02685-x

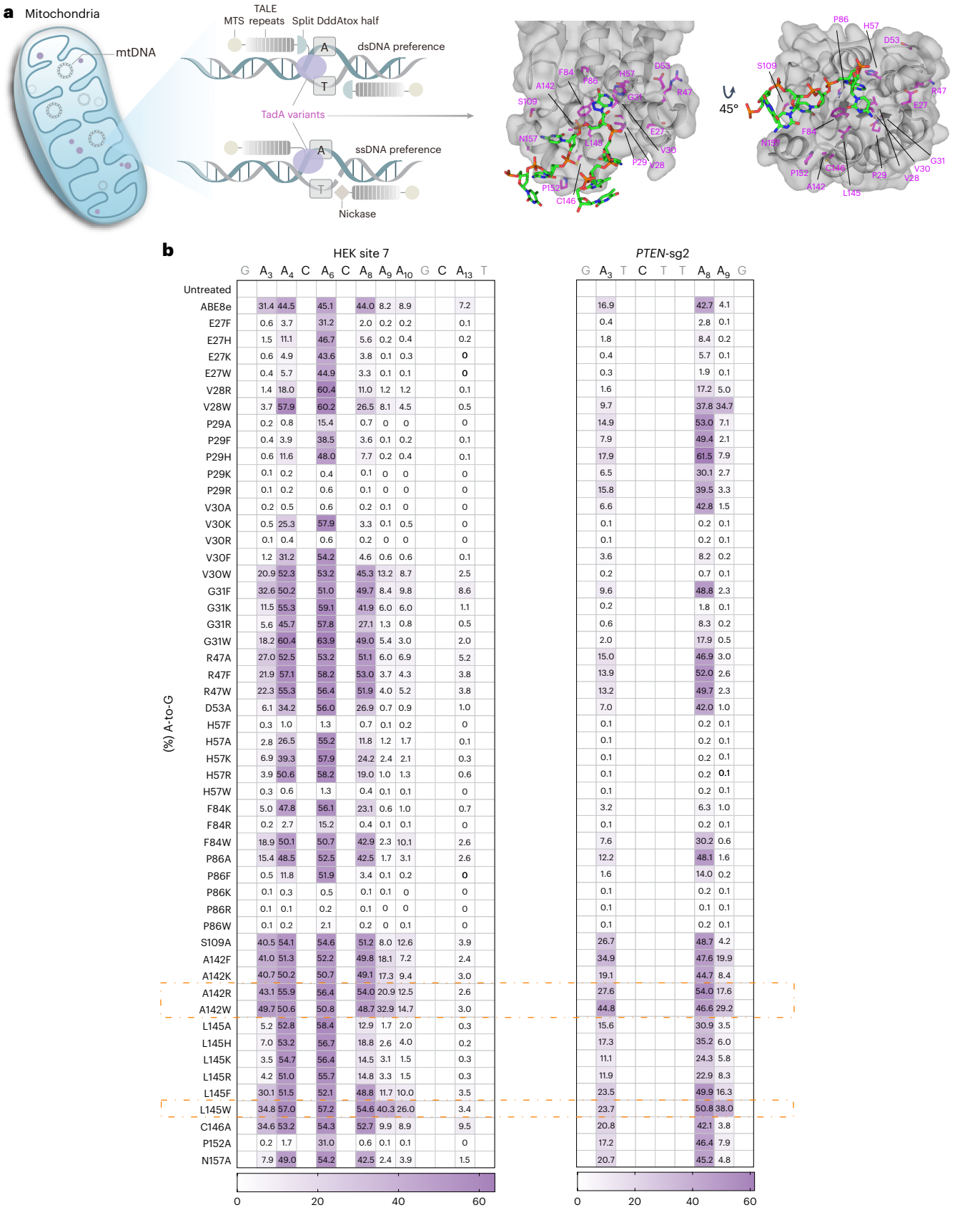

Fig. 1 | Protein engineering of adenine deaminases in CRISPR-based ABEs. **a**, Schematic illustration of eTd-mtABEs using evolved TadA for enhancing dsDNA and ssDNA preferential editing of mitochondria genome. Right, cryo-electron microscopy structure of TadA-8e in complex with the DNA substrate (Protein Data Bank 6VPC). **b**, Heat maps showing nuclear A•T-to-G•C editing efficiencies induced by ABE8e and ABE variants at HEK site 7 and *PTEN*-sg2 in HEK293T cells. The A142R, A142W and L145W substitutions highlighted in orange dotted boxes were chosen for further evaluation. Data represent the mean of three biologically independent experiments.

remains highly challenging, especially without the development of mitochondrial base editors (mitoBEs).

Inspired by CRISPR-based nuclear base-editing strategies, mitoBEs were recently developed by fusing a mitochondrially localized programmable DNA-binding protein module with a nucleotide deaminase moiety to induce targeted base conversions[2,12]. With the identification of double-stranded DNA (dsDNA) cytosine deaminase $DddA_{tox}$, DddA-derived cytosine BEs (DdCBEs) and zinc-finger deaminases were generated through fusion with a uracil glycosylase inhibitor (UGI) and TALE or ZFN DNA recognition moieties[13–20]. By substituting UGI with evolved adenine deaminase (AD) TadA-8e variant, mitochondrial adenine BEs (miABEs) named TALE-linked deaminases (TALEDs) were generated to introduce A•T-to-G•C transitions in both strands of dsDNA[3]. Given that A•T-to-G•C edits theoretically model ~45% and correct ~41% of mtDNA diseases[3,21], miABEs hold immense promise for interrogating the function of mtDNA variants and potentially for mtDNA disease therapeutics. To increase the mtDNA-editing precision, we and other groups have shown that using DNA nickases instead of DddA enhances the strand-preference base conversions but the A•T-to-G•C editing efficiency still has room for improvement[22,23]. A previous study developed improved TALED variants with greatly reduced RNA off-target effects and demonstrated generation of an mtDNA disease mouse model. However, the phenotype of these models is mild, probably because of limited editing efficiency[24]. Most recently, we and other groups demonstrated that using circular RNA-encoded engineered miABEs or fusing human uracil DNA glycosylase to TALEDs can enhance mtDNA base editing in cells or in mice[25,26] because the clinical manifestation of mtDNA diseases often requires heteroplasmy of mtDNA mutation to exceed a high threshold (typically >50%)[5,27]. As a high heteroplasmic mtDNA mutation rate is a prerequisite to mimic mitochondrial disorders, highly efficient mitoBEs are urgently demanded in the field.

In this study, through extensive engineering of TadA-8e, we obtained evolved variants with enhanced editing activity and targeting scope, particularly the RA* (R = A or G) sequence contexts, which are unpreferred targets for TadA-8e. Using these superactive TadA variants, the engineered TadA-derived mtDNA ABEs (eTd-mtABEs) were developed through fusion with split $DddA_{tox}$ modules or nickases guided by TALE arrays and mitochondrial targeting sequences (MTSs) (Fig. 1a). eTd-mtABEs showed enhanced A•T-to-G•C editing frequency comparing to original editors, averaging 6.9-fold (with the TadA-8e-RW variant) or 3.8-fold (with the TadA-8e-RW/V28A variant) in dsDNA-preferred or single-stranded DNA (ssDNA)-preferred targeting, respectively, with an expanded targeting scope and minimized DNA and RNA off-target effects. eTd-mtABEs efficiently installed mtDNA pathogenic point mutations in human cells to model LHON and in rats showing sensorineural hearing loss (SNHL). The development of eTd-mtABEs broadens the spectrum of potential applications and enhances the overall versatility of mitochondrial base-editing technology.

Results

Molecular engineering of ADs

As miABEs induce base conversions less efficiently compared to DdCBEs[3,13], we speculate that the activity of AD is the most critical index for editing efficiency. Inspired by our previous studies and those of others, which showed that the features of activity, specificity and substrate selectivity of TadA deaminase can be substantially amended[28–37], we attempted to further increase its activity through laboratory evolution to ultimately enhance the editing efficiency of miABEs. To evolve a highly efficient TadA variant, CRISPR-based ABE8e was selected as the starting point because of its ease of construction compared to mitoBEs. On the basis of the structure of ABE8e in complex with its substrates[38] (Fig. 1a), the amino acids of TadA-8e involved in substrate recognition or located in or adjacent to the active pocket were individually substituted and the editing efficiency was evaluated at an endogenous target (HEK site 7) with scattered adenosines in variant sequence contexts in HEK293T cells (Fig. 1b).

Firstly, we examined 51 variants constructed by substituting 16 residues to acquire small side chains, aromatic side chains, polarity with positive charges or hydrophobic properties (Fig. 1b). We found that some variants (for example, E27W, V28R, P29F, P86F and P152A) displayed an extremely condensed editing window (A_6) and several variants (for example, V28W, G31W, R47F, A142R and L145W) induced a similar or slightly increased A-to-G efficiency compared to ABE8e in a regular A_4–A_8 (protospacer-adjacent motif sequence as positions 21–23) editing window. Although A_3, A_9 and A_{10} are outside of the canonical editing window, the A142R (43% at A_3, 21% at A_9 and 13% at A_{10}) and A142W (50% at A_3, 33% at A_9 and 15% at A_{10}) variants induced a higher ratio of adenine conversions than ABE8e (31% at A_3, 8% at A_9 and 9% at A_{10}). In addition, the L145W variant also induced a considerable increase in A-to-G events at positions A_9 and A_{10} (40% and 26%) (Fig. 1b and Supplementary Fig. 1a). Similar results were also observed at another target site, demonstrating robust editing activity with average improvements of 1.9-fold and 6.9-fold at A_3 and A_9 for these three variants (A142R, A142W and L145W) (Fig. 1b and Supplementary Fig. 1b,c). We also noticed that, at the evaluated two sites, the activity at all four sequence contexts (NA*, N = A, T, C or G) was increased (Fig. 1b). Therefore, these three variants were selected for further investigation.

Development of enhanced CRISPR-based ABEs

Next, five TadA-8e variant-derived ABEs (A142R, A142W, L145W, A142R/L145W and A142W/L145W) were further characterized at 29 endogenous sites (Fig. 2a). Compared to ABE8e, all constructs exhibited increased base-editing efficiency to some extent. For example, ABE8e-A142W showed up to 40% and 43% A-to-G editing, whereas ABE8e barely edited adenines with frequencies of 2.8% and 7.7% at A_2 and A_8 of *EMX1* site 1, respectively. Higher base conversion rates were induced by ABE8e-A142R/L145W (ABE8e-RW) compared to ABE8e (55% versus 21% at A_9) at another target (*PD1*-sg13). Overall, ABE8e-RW exhibited the highest average editing activity among these five constructs. It showed a dramatic elevation of editing activity at positions A_{-1}–A_3 (averaging 4.9-fold) and A_8–A_{11} (averaging 2.6-fold) in comparison to ABE8e (Fig. 2b,c and Supplementary Fig. 2a). An up to 20-fold increase in adenine conversions was observed for ABE8e-RW at A_{10}. Even within the conventional editing window (A_4–A_7), which is considered nearly saturated in ABE8e[31], the activity of ABE8e-RW exhibited an average 1.2-fold increase (Fig. 2b,c). Previous studies showed that ABEs, including ABE7.10, ABE8s and ABE8e, had a preference for the YA* (Y = T or C) motif context, especially outside the conventional editing window[27,31,32,38,39]. After carefully analyzing A-to-G conversion fold changes at the A_{-1}–A_{11} positions of the above 29 sites, we found that, compared to ABE8e, ABE8e variants (especially A142W and RW) showed enhanced activity in all sequence contexts, with more efficient adenine conversions (up to 4.5-fold on average) in YA* (Y = G or A) motifs, which are considered inefficient contexts for TadA7-derived and TadA8-derived ABEs (Fig. 2d and Supplementary Fig. 2b).

Previous studies demonstrated that ABEs also induce cytosine bystander edits[35,36,40]. Outside of the A142R variant, the other four evolved ABE8e variants only induced minimal indels and very mild cytosine mutations (less than 1.2% on average) compared to ABE8e (less than 2.9% on average) at the evaluated sites (Supplementary Fig. 2c,d). This suggests that the L145 residue is critical for distinguishing between adenine and cytosine substrates and reducing cytosine bystander editing, which is consistent with our previous study[35]. These results indicate that the introduction of substitutions at residues 142 and/or 145 of TadA-8e considerably enhances editing activity and targeting scope and reduces cytosine bystander editing of nuclear ABEs.

Robust mtDNA editing with engineered TadA variants

The dramatically increased deaminase activity and targeting scope of TadA-8e variants encouraged us to investigate their potential for

https://doi.org/10.1038/s41587-025-02685-x

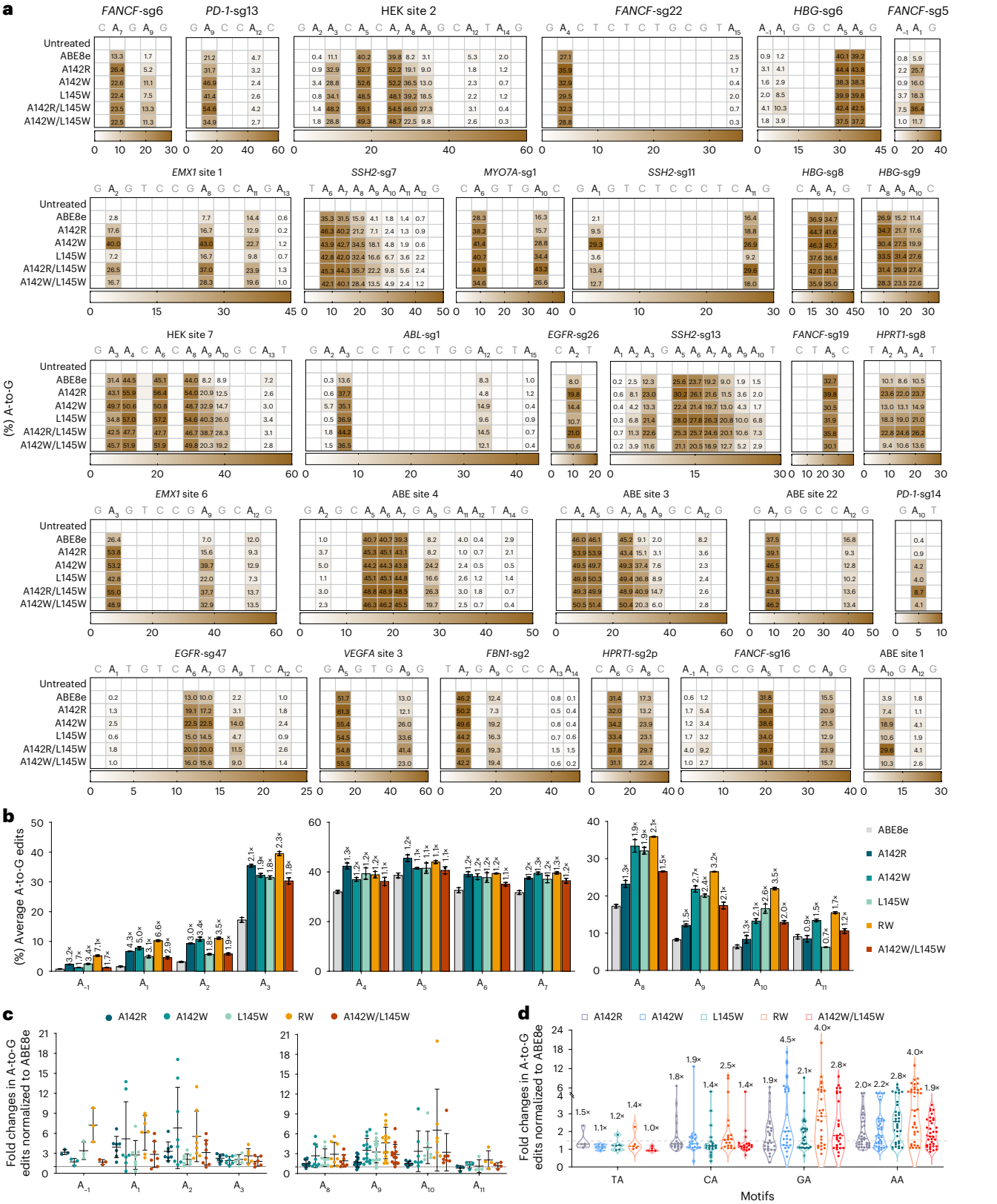

Fig. 2 | Characterization of enhanced CRISPR-derived ABEs. a, Heat maps showing nuclear A-to-G editing efficiencies by indicated ABEs at 29 endogenous target sites in HEK293T cells. Data are shown as the mean from $n = 3$ biologically independent samples. **b**, Average A-to-G edits of indicated ABEs in the protospacer at 29 target sites in **a**. Fold changes of ABE variants versus ABE8e on average A-to-G editing are shown above the bars. Data are shown as the mean ± s.d. from $n = 3$ biologically independent samples. **c**, Dot plot representing fold changes in A-to-G edits of indicated ABEs normalized to ABE8e at positions outside the conventional editing window. Data represent the mean ± s.d. and each dot represents the mean of three biologically independent samples. **d**, Violin plots representing fold changes in A-to-G edits of the indicated ABEs normalized to ABE8e in all sequence contexts (TA, $n = 5$; CA, $n = 20$; GA, $n = 27$; AA, $n = 36$) at 29 endogenous genomic loci in **a**. Average fold changes are shown above each column. Each dot represents the mean of three biologically independent samples.

https://doi.org/10.1038/s41587-025-02685-x

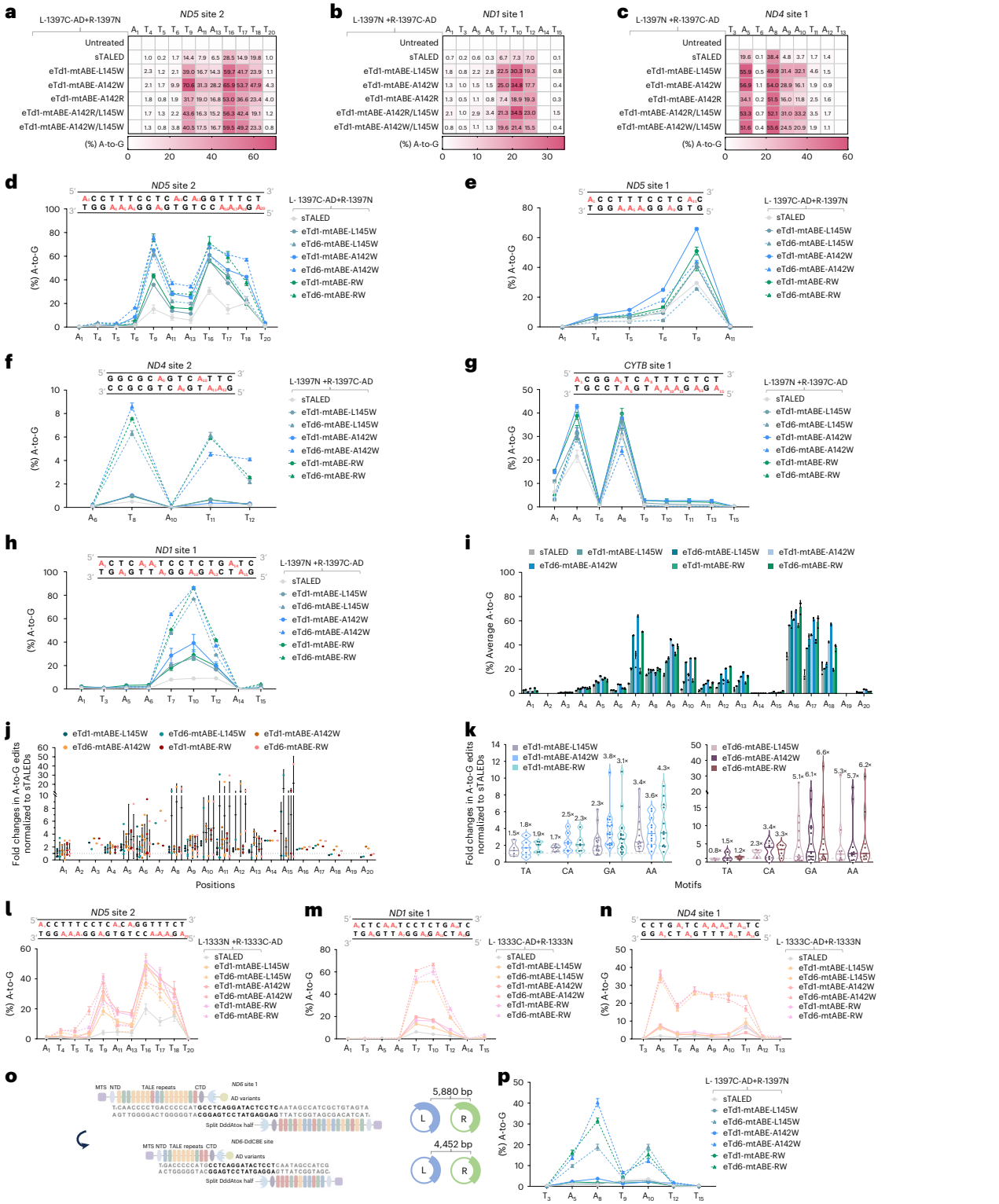

Fig. 3 | Evolved TadA variants improve A•T-to-G•C editing in mtDNA. **a**–**c**, maps showing mitochondrial A•T-to-G•C editing frequencies induced by sTALEDs and eTd1-mtABEs at *ND5* site 2 (**a**), *ND1* site 1 (**b**) and *ND4* site 1 (**c**) in HEK293T cells. Data represent the mean of three biologically independent replicates. **d**–**h**, Editing frequencies of indicated editors at *ND5* site 2 (**d**), *ND5* site 1 (**e**), *ND4* site 2 (**f**), *CYTB* site 1 (**g**) and *ND1* site 1 (**h**) in HEK293T cells. **i**, Average mitochondrial A-to-G editing frequencies induced by indicated eTd-mtABEs. **j**, Fold changes in A-to-G edits mediated by indicated eTd-mtABEs normalized to sTALEDs (dashed line). Data represent the mean ± s.d. and each dot represents the mean of three biologically independent replicates. **k**, Violin plots representing fold changes in A-to-G edits of indicated eTd1-mtABEs (left; TA, $n = 5$; CA, $n = 6$; GA, $n = 17$; AA, $n = 12$) and eTd6-mtABEs (right; TA, $n = 3$; CA, $n = 5$; GA, $n = 15$; AA, $n = 10$) normalized to sTALEDs (dashed line) in all sequence contexts at target sites in **a**–**h**. Average fold changes are shown above each column. Each dot represents the mean of three biologically independent replicates. **l**–**n**, Mitochondrial A-to-G editing of sTALEDs and eTd-mtABEs with $DddA_{tox}$ split at G1333 at *ND5* site 2 (**l**), *ND1* site 1 (**m**) and *ND4* site 1 (**n**) in HEK293T cells. **o**, Left, comparison of *ND6* site 1 and *ND6*-DdCBE site. Right, lengths of coding regions for mitochondrial A-to-G editors using corresponding RVD modules. **p**, Mitochondrial A-to-G editing frequencies of sTALED and eTd-mtABEs at *ND6*-DdCBE site. In **i**,**j**, data were obtained from the five sites in **d**–**h**. In **d**–**i**,**l**–**n**,**p**, data represent the mean ± s.d. of $n = 3$ biologically independent replicates.

mitochondrial A-to-G base editing. The evolved mtDNA ABEs were constructed through fusion of wild-type $DddA_{tox}$ halves split at G1397 and TadA-8e AD variants along with MTSs and TALE arrays (Supplementary Fig. 3a), resulting in a pair of L-1397C-AD/R-1397N or L-1397N/R-1397C-AD variants (eTd1-mtABEs). These eTd1-mtABEs were targeted to three mtDNA sites previously examined with split DddA TALED (sTALED) in HEK293T cells[3]. High-throughput sequencing (HTS) data showed that sTALED (AD in L-TALE) induced A-to-G editing frequencies ranging from 6.5% to 29% at positions 9–18 (the spacer region of two TALE-binding sites) on *ND5* site 2. Notably, all eTd1-mtABEs achieved much higher adenine conversions (14–71%) and the A142W variant was more active than the others (28–71%) at this site (Fig. 3a). Similar results were also obtained from the other construction with AD fused to the R-TALE array and the editing frequency within the same editing window was 52% on average in eTd1-mtABE-A142W-treated cells, whereas sTALED only induced 24% on average (Supplementary Fig. 3b). When targeted to *ND1* site 1, sTALED poorly catalyzed A-to-G conversions (7%) when AD was fused to the R-TALE array, while higher efficiency was observed in the L-1397C-AD construction (26–39%, averaging 34%). Similarly, eTd1-mtABE-RW with the R-TALE (21–35%, averaging 26%) or L-TALE (54–79%, averaging 66%) construction showed a dramatic increase in adenine edits compared to sTALED (Fig. 3b and Supplementary Fig. 3c). In contrast to sTALEDs (averaging 17% editing at *ND4* site 1), all eTd1-mtABEs extended the editing window from A_5–A_8 to A_5–A_{10} while averaging 28–44% editing efficiency regardless of AD locations (Fig. 3c and Supplementary Fig. 3d). In addition to tremendously elevated mtDNA on-target editing efficiency, eTd1-mtABEs showed high product purity and rarely induced indels compared to sTALEDs[3] (Supplementary Fig. 3e–j).

We thought that the recently reported highly active DddA variants[41] might have better ability to unwind mtDNA, which would further improve the efficiency of eTd-mtABE. eTd-mtABEs with the DddA6 variant (eTd6-mtABEs) induced up to 76% A-to-G edits and displayed average improvements of 1.6-fold and 4.3-fold compared to the original eTd1-mtABEs and sTALED at *ND5* site 2, respectively (Fig. 3d), but introduction of the DddA11 variant almost abolished editing activity (Supplementary Fig. 4a). After evaluation of four more targets, we found that the editing frequencies of eTd1-mtABEs and eTd6-mtABEs were much higher (up to 11-fold and 36-fold increases, respectively) than sTALEDs (Fig. 3e–j). However, eTd6-mtABEs were not always more efficient than eTd1-mtABEs. For example, eTd6-mtABEs showed higher efficiency up to 87% at two targets (*ND1* site 1 and *ND4* site 2) but lower efficiency at *CYTB* site 1 and *ND5* site 1 compared to eTd1-mtABEs (Fig. 3e–h). This suggests that the cytosine deaminase activity of DddA variants is probably not necessarily consistent with the DNA-unwinding capability to facilitate TadA deamination. In addition, consistent with the previous study[3] on sTALED, eTd-mtABEs induced very minimal cytosine conversions at the evaluated sites, as C-to-T conversions depend on the presence of UGI in the mitochondria (Supplementary Fig. 4b–f). These data suggest that all eTd1-mtABEs exhibited much higher activity compared to sTALEDs regardless of the location of the evolved deaminase, DddA versions and their split positions. Consistent with the results in nuclear ABE8e variants, eTd-mtABEs showed substantially increased activity in all sequence contexts compared to sTALEDs, especially in the RA* context, where eTd1-mtABEs and eTd6-mtABEs showed up to 4.3-fold and 6.6-fold increases on average (up to 36-fold at a GA motif), respectively, suggesting highly efficient mtDNA A-to-G editing with an expanded targeting scope (Fig. 3k).

Compatibility of TadA variants with diverse constructions

The split orientation of $DddA_{tox}$ is one of the determinants affecting the editing efficiency of mitoBEs and higher mutation rates were achieved using G1333-split $DddA_{tox}$ halves for some targets[3,13]. sTALEDs, eTd1-mtABEs and eTd6-mtABEs with $DddA_{tox}$ split at G1333 were tested at three sites. The average conversion rate of adenines within the spacers of all three targets was 5.4% for the sTALEDs-G1333 construction and higher for the sTALEDs-G1397 construction (13%) (Fig. 3a–c,l–n). Compared to sTALEDs-G1333 (averaging 5.4%), eTd1-mtABEs-G1333 (averaging 15%) and eTd6-mtABEs-G1333 (averaging 32%) catalyzed much higher A-to-G conversions. For example, eTd6-mtABE-A142W and eTd6-mtABE-RW variants showed higher activity (averaging 33% and 34%, respectively) with frequencies up to 67%, even surpassing their counterparts that used DddA-G1397 split orientation at some positions (Fig. 3a–c,l–n).

Given that our TadA-8e variants exhibited exceptionally high activity, we speculated that the superactive deaminase activity would be compatible with shorter TALE arrays and the reduced size would facilitate delivery. TALE arrays of eTd-mtABEs targeting *ND6* site 1 (recognized by 35 RVD modules) and *ND6*-DdCBE site (recognized by 21 RVD modules) were designed to target the same site containing highly similar spacers, as this site was previously tested by mitoBEs with varying lengths of TALE-binding motifs. However, a 1-nt mismatch was introduced in each short TALE array to the *ND6*-DdCBE site as designed previously[3,13,42]. We also observed that the right short TALE array lacked a thymidine (T_0) in the target sequence immediately preceding the RVD[13] (Fig. 3o), the presence of which is critical for TALE-binding activity. When constructed with the conventional 35 RVD modules, sTALEDs induced efficient A-to-G editing, whereas eTd-mtABEs exhibited significantly higher activity (Supplementary Fig. 4g). However, when using 21 RVD modules containing mismatches to the target sequence, sTALEDs nearly lost its activity at this site (<4%). In contrast, eTd-mtABEs, especially eTd6-mtABE-A142W and eTd6-mtABE-RW, induced robust A-to-G conversions with frequencies up to 40% (Fig. 3p). Taken together, these data suggest that TadA variants are very efficient in supporting the fusion of diverse split orientations of $DddA_{tox}$ halves and are compatible for short TALE arrays even with sequence mismatches, which reduces the size by about 25% (~1,400 bp) while achieving efficient editing, indicating an advantage for delivery.

Off-target analysis of evolved mitochondrial A-to-G editors

To profile the off-target activity of eTd-mtABEs, we first evaluated whether they would induce nuclear DNA editing at previously identified sites with similar TALE arrays[3]. Like TALEDs, eTd-mtABEs induced a background level of off-target mutations in the nuclear genome (Supplementary Fig. 5a). Next, mitochondrial whole-genome sequencing (WGS) of HEK293T cells transfected with sTALEDs, eTd-mtABEs and a TALE-free control was performed to test the TALE-independent off-target editing. Compared to sTALEDs, eTd-mtABEs exhibited comparable or slightly increased DNA off-target editing levels without sequence preference (Fig. 4a and Supplementary Fig. 5b,c). Inspired by studies on nuclear ABEs, which showed that substitutions of critical residues increased substrate selectivity and dramatically reduced off-target edits[29–31,34,35,43], we generated 28 constructs combining eTd6-mtABE-A142W or eTd6-mtABE-RW with other variants. After evaluation at two endogenous targets, three constructs (RW/V28A, RW/V106W and V82S/A142W/Q154R) showed consistently comparable or increased A-to-G edits (Fig. 4b). Then, five representative DNA off-target sites identified by the above mitochondrial WGS were used to evaluate the off-target effects of the triple-mutant variants in eTd1-mtABE and eTd6-mtABE constructions. HTS data revealed that all six constructs substantially reduced DNA off-target editing compared to sTALED (Fig. 4c).

A most recent study showed that the original mitochondrial A-to-G editors induced considerable RNA off-target edits[24]. To evaluate this issue, four previously identified high-frequency RNA off-target sites[24] were selected for HTS analysis using four different constructs targeting two endogenous sites (*ND4* site 1 and *ND1* site 1). In contrast to TALEDs, which showed 9–41% RNA off-target editing, all eTd-mtABEs (especially RW;V28A and RW;V106W) induced minimized random RNA off-target editing (Fig. 4d). The above data suggest that these eTd-mtABE variants

https://doi.org/10.1038/s41587-025-02685-x

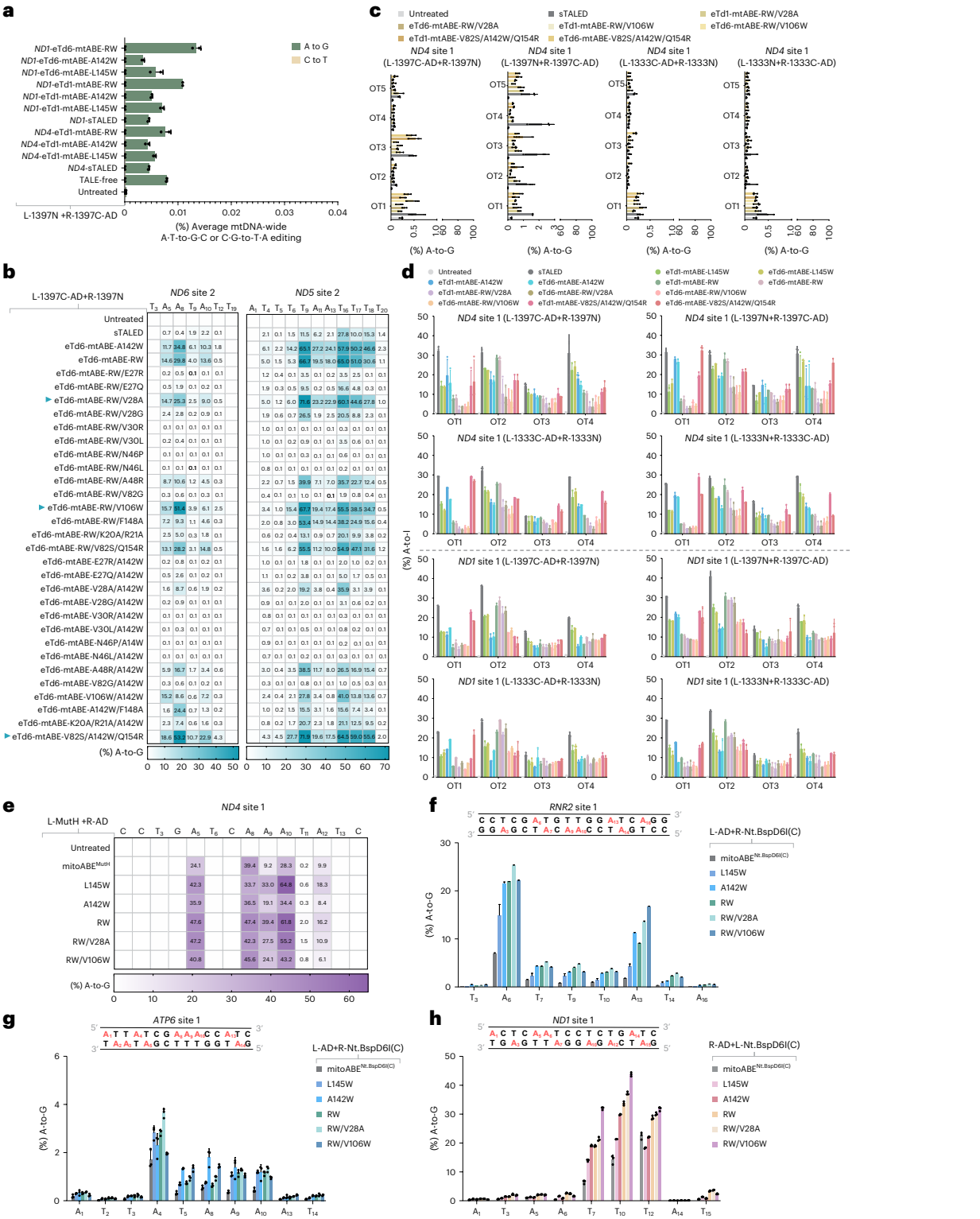

Fig. 4 | TadA variants enhanced specificity of eTd-mtABE and strand-biased mtDNA editing. a, Average percentage of mitochondrial genome-wide off-target editing for sTALEDs and eTd-mtABEs targeting *ND4* and *ND1* sites, respectively. Data represent the mean ± s.d. of $n = 2$ biologically independent replicates. **b**, Comparison of A-to-G efficiencies by sTALED and eTd6-mtABE variants at *ND6* site 2 and *ND5* site 2 in HEK293T cells. eTd6-mtABE variants marked with blue arrows were chosen for further evaluation. Data represent the mean of three biologically independent replicates. **c**, DNA off-target editing frequencies induced by sTALEDs and eTd-mtABEs at five representative DNA off-target sites identified by mitochondrial WGS. **d**, Bar plots showing RNA off-target editing frequencies induced by sTALEDs and eTd-mtABEs at four high-frequency RNA off-target sites identified by transcriptome-wide sequencing. In **c**,**d**, data represent the mean ± s.d. of $n = 3$ independent replicates. **e**, Heat map showing A-to-G editing efficiencies of canonical miABE^{MutH} and miABE^{MutH} constructs with indicated TadA variants at *ND4* site 1 in HEK293T cells. Data represent the mean of three biologically independent replicates. **f**–**h**, A-to-G editing efficiencies of canonical miABE$^{Nt.BspD6I(C)}$ and miABE$^{Nt.BspD6I(C)}$ constructs with indicated TadA variants at *RNR2* site 1 (**f**), *ATP6* site 1 (**g**) and *ND1* site 1 (**h**) in HEK293T cells. Data represent the mean ± s.d. of $n = 3$ independent replicates.

https://doi.org/10.1038/s41587-025-02685-x

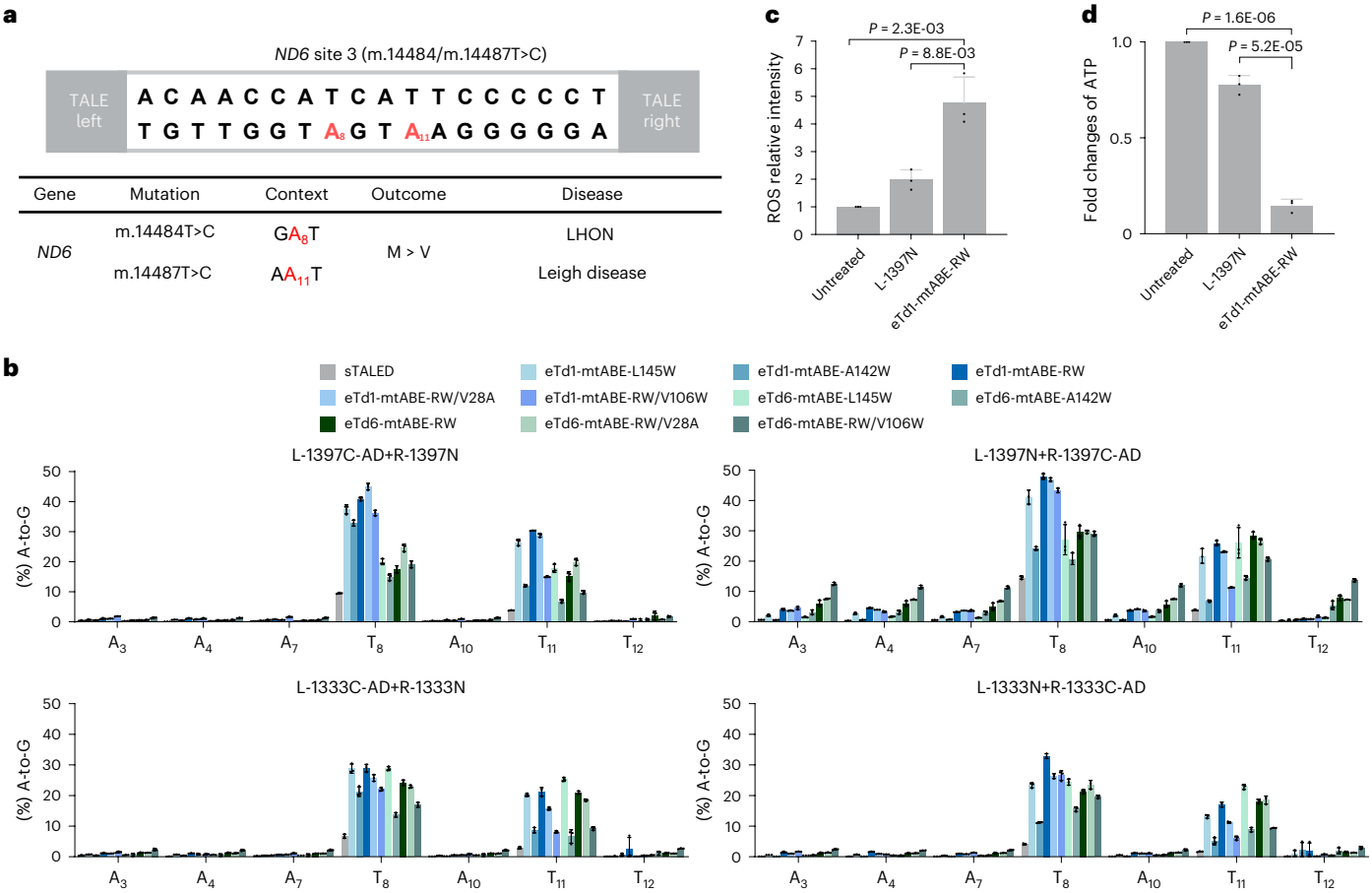

Fig. 5 | Application of eTd-mtABEs to install pathogenic mutations in human cells. a, Application of eTd-mtABEs to install disease-associated mutations in human mtDNA. Two pathogenic mutations located in target spacer region are shown in red. **b**, A-to-G editing frequencies of sTALEDs and eTd-mtABEs with $DddA_{tox}$ split at G1397 or G1333 targeting *ND6* site 3. **c**, The level of intracellular ROS in HEK293T cells treated with L-1397N, eTd1-mtABE-RW (L-1397N + R-1397C-AD) targeting *ND6* site 3. **d**, Fold changes of intracellular ATP in HEK293T cells treated with L-1397N, eTd1-mtABE-RW (L-1397N + R-1397C-AD) targeting *ND6* site 3 using untreated groups as normalized control. In **b**–**d**, data represent the mean ± s.d. of $n = 3$ independent replicates. In **c**,**d**, *P* values were calculated two-tailed Student's *t*-tests.

(especially RW;V28A and RW;V106W) exhibit increased on-target activity but dramatically reduced off-target events compared to sTALED at both DNA and RNA levels.

Enhancing precise mtDNA editing with evolved TadA variants

Recent studies, including ours, demonstrated that fusion of DNA nickases instead of DddA enabled strand-preferred mitochondrial base editing but their limited activity would hinder their applications[3,13,22,23,41]. As the deaminase is a critical limiting component of this system, we supposed that highly efficient TadA variants could enhance their performance. Five engineered TadA variants were individually introduced into $miABE^{MutH}$, a mitochondrial A-to-G editor with specific nicking preferences (5′-GATC-3′) to achieve selective editing at an unnicked mtDNA strand[22]. Editing results at *ND4* site 1 showed that these variants kept the strand-biased editing feature with obviously increased activity. For example, within the editing window (A_5–A_{10}), the TadA-8e-RW variant showed average frequencies of up to 49%, about twofold higher than the original $miABE^{MutH}$ (average of 25%), and the efficiency of the highest editing position was also substantially increased (62% versus 39%) (Fig. 4e). At the hardly edited position for $miABE^{MutH}$ (9.2% at A_9), the RW variant displayed robust A_9-to-G edits (39%). Two precise variants (RW/V28A and RW/V106W) also exhibited very high editing activity comparable to the RW variant. Moreover, the substantial improvement in efficiency by TadA-8e variants was also applicable to $miABE^{Nt.BspD6I(C)}$, which recruits truncated Nt.BspD6I nickase without sequence context constraints[22] (Fig. 4f). Compared to $miABE^{Nt.BspD6I(C)}$, TadA-8e variant-derived editors achieved much higher A-to-G edits with an average improvement of 3.2-fold at all edited adenines of the three tested sites. Even at the highest positions of each site, evolved TadA-8e variants showed more than twofold increases, such as at the highest position of *RNR2* site 1 (25% versus 7%), *ATP6* site 1 (3.7% versus 1.7%) and *ND1* site 1 (44% versus 22%), and kept a low level of undesired editing at the opposite strand (Fig. 4f–h). These results indicate that the evolved TadA-8e variants considerably enhance the efficiency of strand-biased mitochondrial A-to-G editing without affecting editing precision.

Installing pathogenic single-nucleotide variants (SNVs) using eTd-mtABEs in human cells

To test whether eTd-mtABE-induced mtDNA mutations could cause phenotypic effects, we attempted to evaluate the potential of eTd-mtABEs to mimic pathogenic SNVs in human cells. As m.14484T>C and m.14487T>C mutations in the *ND6* gene are implicated in LHON and Leigh syndrome[44–47], respectively, eTd1-mtABEs and eTd6-mtABEs with a G1397 or G1333 orientation were constructed to target *ND6* site 3 covering the pathogenic mutations (Fig. 5a). sTALEDs-G1397 induced less than 15% and 3.8% editing at the desired T_8 and T_{11} positions corresponding to the above pathogenic SNVs and the G1333 orientation showed even lower activity (less than 6.7% and 2.9%, respectively). For instance, the eTd1-mtABE-RW and the accurate eTd1-mtABE-RW;V28A variants supported highly efficient desired T_8 and T_{11} editing with

https://doi.org/10.1038/s41587-025-02685-x

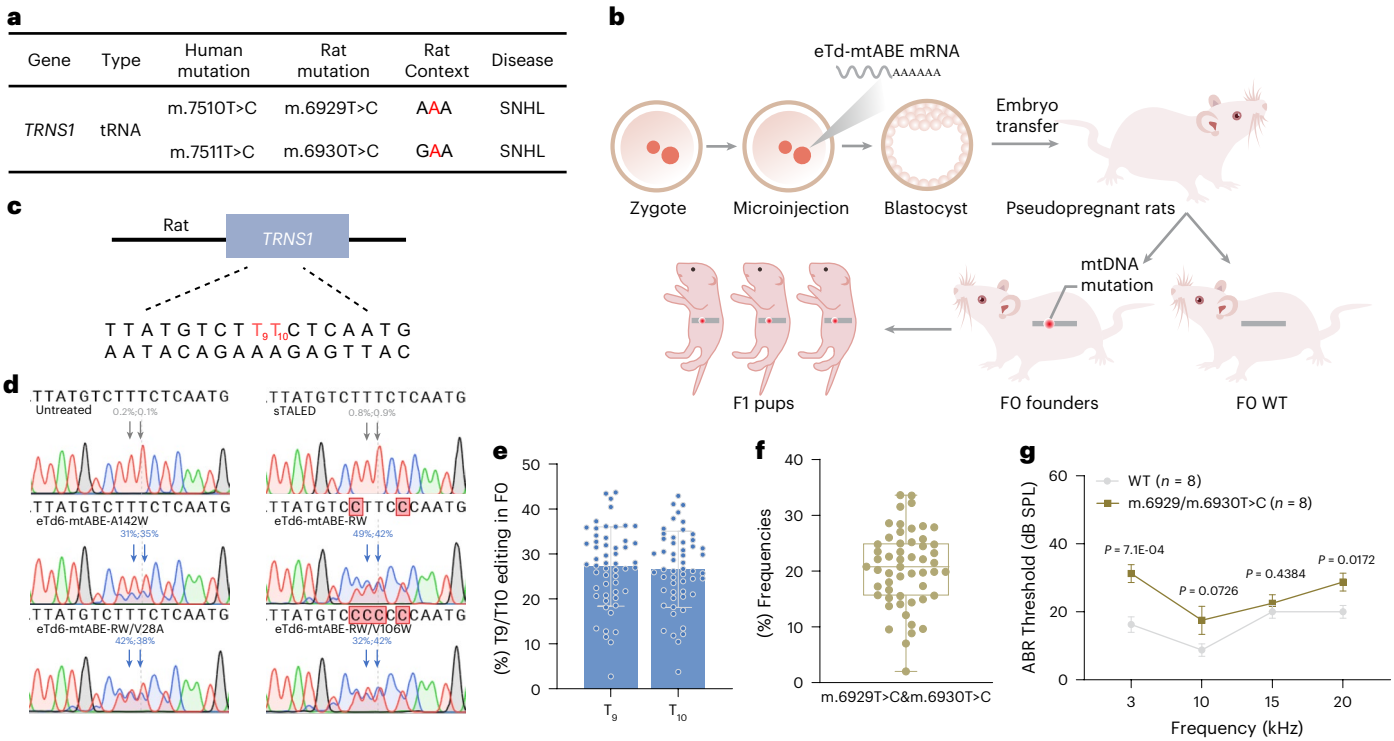

Fig. 6 | Mitochondrial disease models generated by eTd-mtABEs in rats. **a**, Disease-associated mutations in human mtDNA and corresponding rat mtDNA. Pathogenic mutation sites are highlighted in red. **b**, The workflow for eTd-mtABE-mediated generation of disease models in rats carrying pathogenic mutations. **c**, The target sequence of the rat mitochondrial *TRNS1* gene is shown. Two pathogenic mutation sites (T_9 and T_{10}) are highlighted in red. **d**, Sanger sequencing chromatogram of *TRNS1* site 1 edited by indicated editors (L-1333N + R-1333C-AD) in PC12 cells. Arrows indicate the desired editing positions. Data represent the mean of three biologically independent replicates. **e**, Desired T_9-to-C or T_{10}-to-C editing frequencies in F_0 rats. Each data point represents an individual rat ($n = 54$). **f**, Bar plots represent the frequencies of alleles with simultaneous m.6929T>C and m.6930T>C editing. **g**, ABR thresholds of wild-type rats and representative rats with m.6929T>C and m.6930T>C at 4 weeks old. SPL, sound pressure level. Data represent the mean ± s.d. and *P* values were calculated using two-tailed Student's *t*-tests. In **e**,**f**, data represent the mean ± s.d. and each data point represents an individual rat.

either the G1397 orientation (41–48% and 23–30%, respectively) or the G1333 orientation (26–33% and 11–21%, respectively) (Fig. 5b). Although *ND6* site 3 contains an A + T-rich flanking sequence, which is an unfavorable target for TALE binding[48] (Supplementary Fig. 6a), eTd-mtABEs still induced substantially higher editing compared to sTALEDs. In addition, compared to sTALED (3%), up to 26% of edited alleles contained simultaneous m.14484 and m.14487 T-to-C mutations when using eTd1-mtABE-RW, indicating its high activity (Supplementary Fig. 6b,c). Then, we evaluated the phenotypic consequences of these pathogenic SNVs. Compared to untreated cells and cells containing inactive monomer L-1397N, higher levels of reactive oxygen species (ROS) and lower adenosine triphosphate (ATP) levels were observed in cells treated with eTd1-mtABE-RW (Fig. 5c,d). As the cellular phenotype is highly dependent on mtDNA mutation rates, these data suggest that eTd-mtABEs can achieve highly efficient editing to reach the mutation threshold necessary to induce phenotypes in cells, indicating that they are optimal tools for generating cellular models of mitochondrial diseases.

eTd-mtABEs enable mitochondria disease modeling in rats

Animal models of mtDNA diseases are invaluable resources for both basic and translational studies. We attempted to use hyperactive eTd-mtABEs to generate inheritable rat disease models, as the only animal model created by A-to-G conversion associated with mtDNA diseases was generated in mice, albeit with relatively low efficiency[24]. Two pathogenic mtDNA SNVs, m.7510T>C and m.7511T>C mutations in the *TRNS1* gene, cause SNHL[49,50] (Fig. 6a,b and Supplementary Fig. 7a). Firstly, we constructed five eTd-mtABEs along with sTALEDs to target the pathogenic T_9 and T_{10} positions (corresponding to rat m.6929 and m.6930 positions) of *TRNS1* site 1 in PC12 cells (Fig. 6c). In contrast to sTALEDs, which hardly induced the desired T_9 and T_{10} conversions (0.8% and 0.9%, respectively), all eTd-mtABE constructs induced substantially higher base transitions. eTd6-mtABE-RW exhibited superior activity, representing an up to 145-fold increase compared to sTALED, achieving up to 49% and 42% editing at the T_9 and T_{10} positions, respectively (Fig. 6d and Supplementary Fig. 7b). Then, eTd6-mtABE-RW mRNA was injected into rat zygotes; notably, 100% (54/54) of F_0 pups bearing the desired T_9-to-C (averaging 27%, 2.7–44%) and T_{10}-to-C (averaging 27%, 3.8–44%) mutations were obtained (Fig. 6e). Notably, 13 of the founders carried simultaneous pathogenic m.6929 and m.6930 T-to-C mutations with frequencies of over 25% (Fig. 6f and Supplementary Fig. 7c). These pathogenic mutations were efficiently transmitted to the F_1 generation (Supplementary Fig. 7d). Additionally, we observed bystander T_8-to-C editing. Because m.T7510 and m.T7511 (on-target T_9 and T_{10} in *TRNS1*) mutations have been reported to disrupt Watson–Crick base pairing in the acceptor stem of human mt-tRNA^{Ser} (ref. 51), we hypothesized that the editing of T_8 (adjacent to the pathogenic mutation sites and located in the tRNA acceptor arm) could similarly lead to abnormal base pairing, potentially destabilizing the tRNA secondary structure and impairing its function. Auditory brainstem response (ABR) assays across frequencies of 3, 10, 15 and 20 kHz from 4-week-old F_0 founders demonstrated that the ABR thresholds of eight founders were significantly increased at frequencies of 3 and 20 kHz compared to wild-type rats (Fig. 6g), with more severe phenotypes in female founders (Supplementary Fig. 7e). These data demonstrate that eTd-mtABEs can induce robust mtDNA editing in vivo, successfully generating a mitochondrial disease model of SNHL with hearing disorders in rats.

Discussion

MiABEs are crucial tools for mtDNA disease modeling and potentially for gene therapy, as A•T-to-G•C editing can theoretically model and correct over 40% of mtDNA diseases[3,21]. However, this requires a very high ratio of base conversion frequencies (typically >50%)[5,27]. In this study, we evolved hyperactive TadA variants to increase the activity of both nuclear BEs and mitoBEs, especially in noncanonical editing windows and broad sequence contexts.

As TadA deaminases prefer the YA* sequence context, especially outside the major editing window[28,32,33], we believed that this could be an important start point to evolve TadA-8e mutants to reach higher activity. We demonstrated that A142W or A142R;L145W variants could enhance the activity and expand the editing window regardless of sequence context in both nuclear ABEs and miABEs. Our previous study showed that L145 was a critical residue for substrate recognition, as L145T/Q/C substitutions narrowed the editing window and reduced off-target effects and cytosine bystander edits[35]. Here, we found that L145W increased activity but reduced cytosine editing effects (Fig. 2b and Supplementary Fig. 2c). Compared to L145T/Q/C, the bulky substitution of L145W may pack against F84 and adjust L145 to an even more optimal position for deamination. An additional substitution at the nearby position (A142R) may further strengthen the hydrophobic patch created by W145 and F84. Without the L145W substitution, the single A142W substitution may function similarly to L145W. Although TadA7.10 is screened from TA preference targets[28], we demonstrated that extensive evolution can push the deaminase evolving to a broader targeting scope. During the course of our study, an independent group reported the development of TadA8r, which was evolved from wild-type *Escherichia coli* TadA to increase context compatibility in nuclear DNA[52]. The authors considered that the different substitutions at the D108 residue (D108G in TadA8r and D108N in TadA7.10 and TadA-8e descendants) led their BEs to evolve along a distinct trajectory. Our study shows that the D108G substitution is not necessarily required to relax TadA sequence preference and will contribute to the understanding of the working mechanisms of deaminase and further evolution of BEs.

Compared to their original versions, higher adenine conversion activity was observed in miABEs (up to an average of 6.4-fold in the RA* context and 2.4-fold in the YA* context) in comparison to nuclear ABEs (up to an average of 4.0-fold in the RA* context and 1.9-fold in the YA* context) (Figs. 2d and 3k), suggesting that enhancement of deaminase activity is more effective in miABEs. This is probably because of the different mechanisms for exposing the ssDNA substrate by Cas9 and DddA, as Cas9 functions as a helicase and exposes the nontarget strand more thoroughly assisted by single guide RNA (sgRNA)[53,54]. It was evidenced that the evolved DddA6 variant[41], which showed higher activity and an expanded targeting scope in DdCBEs, could further increase base-editing efficiency at some tested sites but not all (Figs. 3e,g and 5b and Supplementary Fig. 4b). Given the more complicated construction of mitoBEs compared to nuclear BEs, it would be important to reveal the underlying rules for generating highly active constructs for specific targets.

Very recently, a V28R variant was identified to reduce the RNA off-targets of sTALEDs but with relatively low on-target activity[24]. In this study, the additional introduction of either V28A or V106W substitutions to eTd-mtABE-RW resulted in a significant decrease in off-target mutations at both DNA and RNA levels (Fig. 4c,d).The accurate version showed increased activity at the tested sites (Fig. 4b) because enhanced precision usually leads to compromised efficiency[35,55]. However, eTd-mtABEs induced base conversion in both mtDNA strands, which increases bystander edits. This problem was partially resolved by our previous study using DNA nickase instead of DddA to induce strand-biased editing[22] and the TadA-8e-RW/V28A variant further increased the activity (Fig. 4e–h), while further improvement of the efficiency of stand-specific editing is highly demanded. eTd-mtABE-RW enabled the highly efficient introduction of pathogenic mutations into rat embryos, allowing for the generation of an SNHL model that can prove invaluable as a resource for both pathological and therapeutic studies. Obvious phenotypes were observed in the F_0 generation with sex-biased defects (Supplementary Fig. 7d). It would be quite interesting to investigate this phenomenon in patients and to further develop treatments on the basis of this model. As demonstrated in recent studies[25,26], modulating the mtDNA repair pathway or using circular RNA-encoded mitoBEs achieved efficient base editing; we speculate that the combination of our TadA variants with these two strategies could further improving A-to-G editing in mtDNA.

The development of eTd-mtABEs advances the utility of mitochondrial base editing for disease modeling and potential therapeutic strategies. Our accompanying study showed the generation of a Leigh syndrome rat model using eTd-mtABE and correction of the pathogenic mutation using engineered DdCBEs in rat embryos[56]. These studies aimed to correct pathogenic point mutations rather than eliminate mutant mtDNA, which would be dangerous in tissues with extremely high levels of mtDNA mutation.

Online content

Any methods, additional references, Nature Portfolio reporting summaries, source data, extended data, supplementary information, acknowledgements, peer review information; details of author contributions and competing interests; and statements of data and code availability are available at https://doi.org/10.1038/s41587-025-02685-x.

References

1. Wallace, D. C. Mitochondrial genetic medicine. *Nat. Genet.* **50**, 1642–1649 (2018).
2. Kim, J. S. & Chen, J. Base editing of organellar DNA with programmable deaminases. *Nat. Rev. Mol. Cell Biol.* **25**, 34–45 (2024).
3. Cho, S. I. et al. Targeted A-to-G base editing in human mitochondrial DNA with programmable deaminases. *Cell* **185**, 1764–177 (2022).
4. Li, G. et al. Gene editing and its applications in biomedicine. *Sci. China Life Sci.* **65**, 660–700 (2022).
5. Silva-Pinheiro, P. & Minczuk, M. The potential of mitochondrial genome engineering. *Nat. Rev. Genet.* **23**, 199–214 (2022).
6. Stewart, J. B. Current progress with mammalian models of mitochondrial DNA disease. *J. Inherit. Metab. Dis.* **44**, 325–342 (2021).
7. Russell, O. M., Gorman, G. S., Lightowlers, R. N. & Turnbull, D. M. Mitochondrial diseases: hope for the future. *Cell* **181**, 168–188 (2020).
8. Bayona-Bafaluy, M. P., Blits, B., Battersby, B. J., Shoubridge, E. A. & Moraes, C. T. Rapid directional shift of mitochondrial DNA heteroplasmy in animal tissues by a mitochondrially targeted restriction endonuclease. *Proc. Natl Acad. Sci. USA* **102**, 14392–14397 (2005).
9. Gammage, P. A. et al. Genome editing in mitochondria corrects a pathogenic mtDNA mutation in vivo. *Nat. Med.* **24**, 1691–1695 (2018).
10. Bacman, S. R. et al. MitoTALEN reduces mutant mtDNA load and restores $tRNA^{Ala}$ levels in a mouse model of heteroplasmic mtDNA mutation. *Nat. Med.* **24**, 1696–1700 (2018).
11. Zekonyte, U. et al. Mitochondrial targeted meganuclease as a platform to eliminate mutant mtDNA in vivo. *Nat. Commun.* **12**, 3210 (2021).
12. Rees, H. A. & Liu, D. R. Base editing: precision chemistry on the genome and transcriptome of living cells. *Nat. Rev. Genet.* **19**, 770–788 (2018).
13. Mok, B. Y. et al. A bacterial cytidine deaminase toxin enables CRISPR-free mitochondrial base editing. *Nature* **583**, 631–637 (2020).

14. Huang, J. et al. Discovery of deaminase functions by structure-based protein clustering. *Cell* **186**, 3182–3195 (2023).
15. Mi, L. et al. DddA homolog search and engineering expand sequence compatibility of mitochondrial base editing. *Nat. Commun.* **14**, 874 (2023).
16. Guo, J. et al. A DddA ortholog-based and transactivator-assisted nuclear and mitochondrial cytosine base editors with expanded target compatibility. *Mol. Cell* **83**, 1710–1724 (2023).
17. Sun, H. et al. Developing mitochondrial base editors with diverse context compatibility and high fidelity via saturated spacer library. *Nat. Commun.* **14**, 6625 (2023).
18. Lim, K., Cho, S. I. & Kim, J. S. Nuclear and mitochondrial DNA editing in human cells with zinc finger deaminases. *Nat. Commun.* **13**, 366 (2022).
19. Willis, J. C. W., Silva-Pinheiro, P., Widdup, L., Minczuk, M. & Liu, D. R. Compact zinc finger base editors that edit mitochondrial or nuclear DNA in vitro and in vivo. *Nat. Commun.* **13**, 7204 (2022).
20. Lee, S., Lee, H., Baek, G. & Kim, J. S. Precision mitochondrial DNA editing with high-fidelity DddA-derived base editors. *Nat. Biotechnol.* **41**, 378–386 (2023).
21. Phan, H. T. L., Lee, H. & Kim, K. Trends and prospects in mitochondrial genome editing. *Exp. Mol. Med.* **55**, 871–878 (2023).
22. Yi, Z. et al. Strand-selective base editing of human mitochondrial DNA using mitoBEs. *Nat. Biotechnol.* **42**, 498–509 (2024).
23. Hu, J. et al. Strand-preferred base editing of organellar and nuclear genomes using CyDENT. *Nat. Biotechnol.* **42**, 936–945 (2024).
24. Cho, S. I. et al. Engineering TALE-linked deaminases to facilitate precision adenine base editing in mitochondrial DNA. *Cell* **187**, 95–109 (2024).
25. Zhang, X. et al. Precise modelling of mitochondrial diseases using optimized mitoBEs. *Nature* **639**, 735–745 (2025).
26. Fan, Y. et al. Leveraging base excision repair for efficient adenine base editing of mitochondrial DNA. *Nat. Biotechnol.* https://doi.org/10.1038/s41587-025-02608-w (2025).
27. Gorman, G. S. et al. Mitochondrial diseases. *Nat. Rev. Dis. Primers* **2**, 16080 (2016).
28. Gaudelli, N. M. et al. Programmable base editing of A*T to G*C in genomic DNA without DNA cleavage. *Nature* **551**, 464–471 (2017).
29. Zhou, C. et al. Off-target RNA mutation induced by DNA base editing and its elimination by mutagenesis. *Nature* **571**, 275–278 (2019).
30. Grunewald, J. et al. CRISPR DNA base editors with reduced RNA off-target and self-editing activities. *Nat. Biotechnol.* **37**, 1041–1048 (2019).
31. Rees, H. A., Wilson, C., Doman, J. L. & Liu, D. R. Analysis and minimization of cellular RNA editing by DNA adenine base editors. *Sci. Adv.* **5**, eaax5717 (2019).
32. Richter, M. F. et al. Phage-assisted evolution of an adenine base editor with improved Cas domain compatibility and activity. *Nat. Biotechnol.* **38**, 883–891 (2020).
33. Gaudelli, N. M. et al. Directed evolution of adenine base editors with increased activity and therapeutic application. *Nat. Biotechnol.* **38**, 892–900 (2020).
34. Chen, L. et al. Re-engineering the adenine deaminase TadA-8e for efficient and specific CRISPR-based cytosine base editing. *Nat. Biotechnol.* **41**, 663–672 (2023).
35. Chen, L. et al. Engineering a precise adenine base editor with minimal bystander editing. *Nat. Chem. Biol.* **19**, 101–110 (2023).
36. Jeong, Y. K. et al. Adenine base editor engineering reduces editing of bystander cytosines. *Nat. Biotechnol.* **39**, 1426–1433 (2021).
37. Tu, T. et al. A precise and efficient adenine base editor. *Mol. Ther.* **30**, 2933–2941 (2022).
38. Lapinaite, A. et al. DNA capture by a CRISPR-Cas9-guided adenine base editor. *Science* **369**, 566–571 (2020).
39. Arbab, M. et al. Determinants of Base Editing Outcomes from Target Library Analysis and Machine Learning. *Cell* **182**, 463–480 e430 (2020).
40. Kim, H. S., Jeong, Y. K., Hur, J. K., Kim, J. S. & Bae, S. Adenine base editors catalyze cytosine conversions in human cells. *Nat. Biotechnol.* **37**, 1145–1148 (2019).
41. Mok, B. Y. et al. CRISPR-free base editors with enhanced activity and expanded targeting scope in mitochondrial and nuclear DNA. *Nat. Biotechnol.* **40**, 1378–1387 (2022).
42. Bacman, S. R. et al. Specific elimination of mutant mitochondrial genomes in patient-derived cells by mitoTALENs. *Nat. Med.* **19**, 1111–1113 (2013).
43. Yan, D. et al. High-efficiency and multiplex adenine base editing in plants using new TadA variants. *Mol. Plant* **14**, 722–731 (2021).
44. Catarino, C. B. et al. Characterization of a Leber's hereditary optic neuropathy (LHON) family harboring two primary LHON mutations m.11778G>A and m.14484T>C of the mitochondrial DNA. *Mitochondrion* **36**, 15–20 (2017).
45. Macmillan, C. et al. Pedigree analysis of French Canadian families with T14484C Leber's hereditary optic neuropathy. *Neurology* **50**, 417–422 (1998).
46. Thorburn, D. R., Rahman, J., and Rahman, S. Mitochondrial DNA-Associated Leigh Syndrome and NARP. In GeneReviews((R)), M. P. Adam, J. Feldman, G. M. Mirzaa, R. A. Pagon, S. E. Wallace, L. J. H. Bean, K. W. Gripp, and A. Amemiya, eds. (1993).
47. Khoo, A. et al. Progressive myoclonic epilepsy due to rare mitochondrial ND6 mutation, m.14487T>C. *BMJ Neurol. Open* **3**, e000180 (2021).
48. Becker, S. & Boch, J. TALE and TALEN genome editing technologies. *Gene and Genome Editing* **2**, 100007 (2021).
49. Kytovuori, L., Gardberg, M., Majamaa, K. & Martikainen, M. H. The m.7510T>C mutation: Hearing impairment and a complex neurologic phenotype. *Brain Behav.* **7**, e00859 (2017).
50. Mutai, H., Watabe, T., Kosaki, K., Ogawa, K. & Matsunaga, T. Mitochondrial mutations in maternally inherited hearing loss. *BMC Med. Genet* **18**, 32 (2017).
51. Ding, Y. et al. The role of mitochondrial DNA mutations in hearing loss. *Biochem. Genet.* **51**, 7–8 (2013).
52. Xiao, Y. L., Wu, Y. & Tang, W. An adenine base editor variant expands context compatibility. *Nat. Biotechnol.* **42**, 1442–1453 (2024).
53. Jiang, F. & Doudna, J. A. CRISPR-Cas9 Structures and Mechanisms. *Annu. Rev. Biophys.* **46**, 505–529 (2017).
54. Yin, L., Shi, K. & Aihara, H. Structural basis of sequence-specific cytosine deamination by double-stranded DNA deaminase toxin DddA. *Nat. Struct. Mol. Biol.* **30**, 1153–1159 (2023).
55. Kim, Y. B. et al. Increasing the genome-targeting scope and precision of base editing with engineered Cas9-cytidine deaminase fusions. *Nat. Biotechnol.* **35**, 371–376 (2017).
56. Chen, L. et al. A mitochondrial disease model is generated and corrected using engineered base editors in rat zygotes. *Nat. Biotechnol.* https://doi.org/10.1038/s41587-025-02684-y (2025).

[1]Shanghai Frontiers Science Center of Genome Editing and Cell Therapy, Shanghai Key Laboratory of Regulatory Biology, School of Life Sciences, East China Normal University, Shanghai, China. [2]Lingang Laboratory, Shanghai, China. [3]School of Pharmacy, East China Normal University, Shanghai, China. [4]Key Laboratory of Brain Functional Genomics of Ministry of Education, Shanghai Key Laboratory of Brain Functional Genomics, School of Life Sciences, East China Normal University, Shanghai, China. [5]New York University-East China Normal University Institute of Brain and Cognitive Science, New York University, Shanghai, Shanghai, China. [6]School of Life Science and Technology, ShanghaiTech University, Shanghai, China. [7]BRL Medicine, Inc., Shanghai, China. [8]Biomedical Pioneering Innovation Center, Peking-Tsinghua Center for Life Sciences, Peking University Genome Editing Research Center, State Key Laboratory of Protein and Plant Gene Research, School of Life Sciences, Peking University, Beijing, China. [9]Changping Laboratory, Beijing, China. [10]Shanghai Academy of Natural Sciences (SANS), Shanghai, China. [11]These authors contributed equally: Liang Chen, Mengjia Hong, Changming Luan. ✉e-mail: chenliang@lglab.ac.cn; dlli@bio.ecnu.edu.cn

Methods

Plasmid construction

The primers used in this study are listed in Supplementary Table 1. Oligonucleotides are listed in Supplementary Table 2. Amino acid and nucleotide sequences are listed in Supplementary Table 3. The primers and oligonucleotides were synthesized by BioSune. TALED_Left-ND1-1397C-AD (183892), TALED_Right-ND1-1397N (183898), ND4-DdCBE-left side TALE (157844), ND4-DdCBE-right side TALE (157843), ND4.2-Left TALE-G1397-N-DddA11-mCherry (179682), ND4.2-Right DdCBE-G1397-C-T1413I-GFP (179686) and ABE8e (138489) plasmids were purchased from Addgene. New nuclear BE and mitoBE plasmids were constructed using previously published methods[57,58]. In brief, DNA fragments were amplified using PrimeSTAR Max DNA polymerase (Takara) and assembled with a ClonExpress MultiS one-step cloning kit (Vazyme) according to the manufacturer's protocol. TadA-8e variants with individual or combinational substitutions were constructed by site-directed mutagenesis using a PCR-based method. For nuclear base editing, sgRNAs were constructed by annealing from 95 °C down to room temperature and ligating into BbsI-linearized U6-sgRNA(sp)-EF1α-GFP (Thermo Fisher Scientific). For double-strand mtDNA editing, we firstly construct the original eTd-mtABE expression plasmids (the TALE array was replaced with two inverted BsmBI restriction sites) and assembled the TALE array using Golden Gate (New England Biolabs). All TALE array sequences are listed in Supplementary Table 2. eTd-mtABEs were replaced by TadA-8e and DddAtox variants based on sTALEDs. For stand-preferred mtDNA editing, human codon-optimized MutH and Nt.BspD6I(C) were synthesized (Genewiz). The miABE expression plasmids were constructed by fusing MutH/Nt.BspD6I(C) or TadA-8e variants to the C terminus of TALE[22]. For flow cytometry assays, double-stranded or stand-preferred mtDNA-editing constructs were modified with mCherry or GFP using a P2A sequence. Plasmids were transformed into DH5α chemically competent cells (TransGen Biotech). Plasmids used for transfection were isolated using the Tiangen plasmid mini extraction kit according to the manufacturer's instructions.

Cell culture and transfection

Human HEK293T cells (American Type Culture Collection (ATCC), CRL-3216) and rat PC12 cells (ATCC, CRL-1721) were cultured in DMEM (Gibco) supplemented with 10% (v/v) FBS (Gibco) and 1% (v/v) penicillin and streptomycin. All cell types were maintained at 37 °C with 5% CO_2. HEK293T cells were passaged every 2 or 3 days and PC12 cells were passaged every 3 or 4 days. For nuclear base editing, HEK293T cells were seeded in 24-well plates (Corning) and transfected with 750 ng of nuclear BE plasmids and 250 ng of sgRNA plasmids at 70–80% confluence using polyethyleneimine (PEI; Polysciences). For evaluating the mitochondrial base editing, HEK293T cells were seeded in 12-well plates (Corning) and transfected with 800 ng of eTd-mtABE, sTALED or miABE monomer at 70–80% confluence using PEI (Polysciences). PC12 cells were seeded in 12-well plates (Corning) and transfected with 1,600 ng of eTd-mtABE or TALED monomer at 70–80% confluence using Lipofectamine LTX (Thermo Fisher Scientific).

Genomic DNA extraction and amplification

To assess nuclear base-editing efficiency, HEK293T cells transfected after 72 h were washed with 1× PBS, trypsinized and collected by centrifugation for genomic DNA extraction. To evaluate mitochondrial base-editing efficiency, HEK293T cells or PC12 cells transfected after 72 h were washed with 1× PBS and digested with 0.25% trypsin (Gibco) for fluorescence-activated cell sorting (FACS). EGFP and mCherry double-positive cells were harvested and the genomic DNA was extracted using QuickExtract DNA extraction solution (Lucigen) according to the manufacturer's recommended protocol. The extraction solution was incubated at 65 °C for 6 min and then 98 °C for 2 min. To obtain the genotype of modified rat, genomic DNA for PCR was extracted from collected tissues using the traditional isopropyl method. Genome loci of interest were amplified with site-specific primers listed in Supplementary Table 1 using KOD-Plus-Neo DNA polymerase (Toyobo).

Mitochondrial WGS

To evaluate the specificity of eTd-mtABEs across the whole mitochondrial genome, HEK293T cells were seeded in 12-well plates (Corning) and transfected with 800 ng of eTd-mtABE or sTALED monomer at 70–80% confluence using PEI. HEK293T cells transfected after 72 h were washed with 1× PBS, trypsinized and collected by centrifugation at 800*g*, 4 °C. The mitochondria were isolated from transfected cells using the mitochondria isolation kit for cultured cells (Thermo Fisher Scientific) according to the manufacturer's protocol. mtDNA was extracted from isolated mitochondria using the TIANamp genomic DNA kit. Long-range PCR was amplified by PrimeSTAR GXL polymerase (Takara) using two sets of partially overlapping primers (listed in Supplementary Table 1) to capture the whole mtDNA genome. PCR products were purified using HiPure gel pure micro kit (Magen Biotech). Subsequently, the WGS was performed at the mean coverage of 13,151× using the Illumina NovaSeq 6000 platform (Genewiz). Regions of interest were amplified by PCR with site-specific primers listed in Supplementary Table 1.

RNA purification and targeted RNA sequencing

HEK293T cells were seeded in 12-well plates (Corning) and transfected with 800 ng of eTd-mtABE or sTALED monomer using PEI. Cells transfected after 72 h were washed with 1× PBS, trypsinized and collected by centrifugation at 800*g*, 4 °C. Collected cells were then homogenized in TRIzol reagent (Magen Biotech). Total RNA was extracted using standard methods and then reverse-transcribed into complementary DNA (cDNA) using Hifair II first-strand cDNA synthesis supermix (Yeasen) according to the manufacturer's protocol. Genome loci of interest were amplified with site-specific primers listed in Supplementary Table 1.

Intracellular ROS assay

Intracellular ROS was measured using an ROS assay kit (Beyotime Biotech) following the manufacturer's instructions. The DCFH-DA probe was diluted to a final concentration of 10 μM and Rosup served as the positive control. HEK293T cells were seeded in 12-well plates (Corning) and transfected with 800 ng of eTd-mtABE monomer or L-1397N using PEI. After 72 h, the medium was removed and the cells were washed three times with PBS. The staining method was conducted according to the instructions. In brief, HEK293T cells were incubated with diluted DCFH-DA probe for 5 min at 37 °C and detected through flow cytometry using a BD Fortessa flow cytometer (BD Biosciences).

ATP assay

ATP was measured using an enhanced ATP assay kit (Beyotime Biotech) following the manufacturer's instructions. HEK293T cells were seeded in six-well plates (Corning) and transfected with 800 ng of eTd-mtABE or L-1397N using PEI. The transfected cells after 72 h were washed with 1× PBS and digested with 0.25% trypsin (Gibco) for FACS. About 1,000,000 EGFP and mCherry double-positive cells were harvested and immediately lysed in 200 μl of lysis buffer on ice. The protein concentration of each treated group was determined using the Pierce BCA protein assay kit (Thermo Fisher Scientific). In a 96-well plate, 20 μl of supernatant was added into wells containing 100 μl of ATP detection working reagent. The plate was then incubated at room temperature for 5 min. The luminescence was detected using an EnVision multilabel reader and the total ATP levels were defined in nmol mg^{-1}.

mRNA preparation

In vitro transcription (IVT) template DNAs were prepared by linearizing with EcoRI and extracted using the phenol–chloroform method. mRNAs were synthesized using Hi-Yield T7 IVT reagent (N1-Me-pUTP) (Hzymes) according to the manufacturer's protocol. In brief, after 2-h incubation at 37 °C, 1 µl of DNase I was added into the solution and incubated at 37 °C for 15 min to digest the template DNA. Subsequently, the IVT reaction solution was purified by ammonium acetate and washed with precooled 70% ethanol. mRNA was eluted in RNase-free water (Takara) and stored at −80 °C.

Animals and microinjection of zygotes

Sprague–Dawley rats used in this study were purchased from Shanghai Jihui Textile Technology. Rats were maintained in specific-pathogen-free facilities at 20–22 °C with 40–60% humidity under a 12-h light–dark cycle. All animal experiments met the regulations drafted by the Association for Assessment and Accreditation of Laboratory Animal Care in Shanghai and were approved by the Experimental Animal Welfare Ethics Committee of East China Normal University (ECNU; license number R20241214). Animal manipulations were in line with previous reports[35,59]. The mixture of eTd-mtABE-encoding mRNAs (150 ng μl^{-1} each) was diluted in RNase-free water and injected into the cytoplasm using an Eppendorf TransferMan NK2 micromanipulator. Injected zygotes were transferred into pseudopregnant female rats at 7–8 weeks old.

ABR measurement

The ABR measurements were consistent with a previous report in a shielded, double-walled sound room[60]. Rats were anesthetized with an intraperitoneal injection of pentobarbitone (50 mg kg^{-1} body weight) and three electrodes were inserted into the subcutaneous tissues at the scalp midline (the recording electrode), posterior to the stimulated ear (the reference electrode) and on the midline of the back 1–2 cm posterior to the neck of the animal (the ground electrode). Tone pips (3, 10, 15 and 20 kHz) at different intensities were generated and delivered using TDT System III (Tucker-Davis Technologies) to test the frequency-specific hearing thresholds. Each sound stimulus was played 20 times per second for 10 s and passed through the sound guide tube into the rat's external ear canal. The ABR signals were acquired, filtered, amplified and analyzed using equipment and software (BioSig) manufactured by Tucker-Davis Technologies. The ABR threshold was defined as the lowest sound intensity capable of eliciting a response pattern characteristic of that observed at higher intensities. The animal's body temperature was monitored using a rectal probe and maintained at ~37 °C by a feedback-controlled heating blanket.

Next-generation sequencing and data analysis

The second PCR amplifications were performed with primers containing an adaptor sequence (forward, 5′-GGAGTGAGTACGGTGTGC-3′; backward, 5′-GAGTTGGATGCTGGATGG-3′) and diverse barcode sequences at the 5′ end. The resulting HTS libraries were pooled and purified by electrophoresis with a 1.5% agarose gel using the HiPure gel pure DNA micro kit (Magen) eluting with 60 µl of H_2O and then sequenced on an Illumina HiSeq platform. To assess base-editing efficiencies, A•T-to-G•C efficiencies and indels in the HTS data were analyzed using BE-Analyzer[61]. Base-editing efficiencies were calculated as the base substitution reads divided by total reads. Purities were calculated as the percentage of the reads of A•T-to-G•C edits divided by the reads of adenine edits without indels. Indel frequencies were calculated as the percentage of reads of indels divided by total reads.

Analysis of mitochondrial genome-wide off-target editing

The analysis of mitochondrial WGS data was performed as previously reported[3]. Initially, we aligned the FASTQ sequences to the GRCh38 (release version 102) reference genome using BWA (version 0.7.17) and then created BAM files with SAMtools (version 1.9) by fixing read=pairing information and flags. Subsequently, we used the REDItoolDenovo.py script from REDItools (version 1.2.1) to find all thymines and adenines in the mitochondrial genome with conversion rates > 0.1%. Positions with conversion rates ≥ 10% in both treated and untreated samples were identified as SNVs in the cell lines and removed. We also excluded the construct's on-target sites. The remaining sites were regarded as off-target sites and we counted the number of edited A or T nucleotides with editing frequencies > 0.1%. We calculated the average A•T-to-G•C editing frequency for all bases in the mitochondrial genome by averaging the conversion rates at each base location in the off-target sites. Average mtDNA-wide A-to-G editing frequency was calculated as the percentage of the sum of A•T-to-G•C off-target sites divided by all bases in the mitochondrial genome. Average mtDNA-wide C-to-T editing frequency was calculated as the percentage of the sum of C•G-to-T•A off-target sites divided by all bases in the mitochondrial genome. Mitochondrial genome-wide graphs were constructed by plotting the conversion rates at on-target and off-target sites with an editing frequency ≥ 1% across the entire mitochondrial genome.

Statistical analysis and reproducibility

Data are presented as the mean ± s.d. from independent experiments. All statistical analyses were performed on $n = 3$ biologically independent experiments, unless otherwise noted in the figure captions, using GraphPad Prism version 9.3.1 software.

Reporting summary

Further information on research design is available in the Nature Portfolio Reporting Summary linked to this article.

Data availability

HTS data were deposited to the National Center for Biotechnology Information (NCBI) Sequence Read Archive (SRA) database under BioProjects PRJNA1249660, PRJNA1249952 and PRJNA1249944. Mitochondrial WGS data were deposited to the NCBI SRA database under BioProject PRJNA1249252. There are no restrictions on data availability. Source data are provided with this paper.

References

57. Chen, L. et al. Adenine transversion editors enable precise, efficient A•T-to-C•G base editing in mammalian cells and embryos. *Nat. Biotechnol.* **42**, 638–650 (2024).
58. Zhang, X. et al. Increasing the efficiency and targeting range of cytidine base editors through fusion of a single-stranded DNA-binding protein domain. *Nat. Cell Biol.* **22**, 740–750 (2020).
59. Chen, Y. et al. Generation of obese rat model by transcription activator-like effector nucleases targeting the leptin receptor gene. *Sci. China Life Sci.* **60**, 152–157 (2017).
60. Cheng, Y. et al. Degraded cortical temporal processing in the valproic acid-induced rat model of autism. *Neuropharmacology* **209**, 109000 (2022).
61. Hwang, G. H. et al. Web-based design and analysis tools for CRISPR base editing. *BMC Bioinformatics* **19**, 542 (2018).

Acknowledgements

We thank Y. Zhang from the Flow Cytometry Core Facility of School of Life Sciences at ECNU and acknowledge the support from the ECNU public platform for innovation (011). We thank L. Ji (HAVAS) for designing schematic diagrams. This work was partially supported by grants from the National Natural Science Foundation of China (32025023, 32230064

and 32311530111 to D.L.; 31930016 to W.W.; 82230002 to M.L.), National Key R&D Program of China (2024YFC3407900 to L.C.; 2023YFC3403400 to D.L.), Shanghai Municipal Commission for Science and Technology (21JC1402200 and 24J22800400 to D.L.), Young Elite Scientist Sponsorship Program by China Association for Science and Technology (2023QNRC001 to L.C.), Shanghai Oriental Talent Plan (QNZH2024131 to L.C.), Fellowship of China Postdoctoral Science Foundation (8206400139 to Z.Y.) and Lingang Laboratory. D.L. is a Shanghai Academy of Natural Sciences exploration scholar.

Author contributions

L.C. and D.L. designed the experiments. L.C., M.H., C.L., M.Y., Y.W., X.G., Y.F., H.H., X.D., H.G., X.C. and L.G. performed the experiments. L.C., M.H., C.L., M.Y., X.G., Y.F., H.H., X.D., D.Z., D.M., M.H., Z.Y., M.L., G.S., X.Z., W.W. and D.L. analyzed the data. L.C. and D.L. wrote the manuscript with input from all authors. L.C. and D.L. supervised the research.

Competing interests

The authors have submitted patent applications based on the results reported in this study (L.C., D.L., M.H. and C.L.). The remaining authors declare no competing interests.

Additional information

Supplementary information The online version contains supplementary material available at https://doi.org/10.1038/s41587-025-02685-x.

Correspondence and requests for materials should be addressed to Liang Chen or Dali Li.

Peer review information *Nature Biotechnology* thanks the anonymous reviewers for their contribution to the peer review of this work.

nature portfolio

Corresponding author(s): Liang Chen, Dali Li

Last updated by author(s): Apr 16, 2025

Reporting Summary

Nature Portfolio wishes to improve the reproducibility of the work that we publish. This form provides structure for consistency and transparency in reporting. For further information on Nature Portfolio policies, see our Editorial Policies and the Editorial Policy Checklist.

Statistics

For all statistical analyses, confirm that the following items are present in the figure legend, table legend, main text, or Methods section.

n/a	Confirmed
☐	☒ The exact sample size (*n*) for each experimental group/condition, given as a discrete number and unit of measurement
☐	☒ A statement on whether measurements were taken from distinct samples or whether the same sample was measured repeatedly
☐	☒ The statistical test(s) used AND whether they are one- or two-sided *Only common tests should be described solely by name; describe more complex techniques in the Methods section.*
☒	☐ A description of all covariates tested
☒	☐ A description of any assumptions or corrections, such as tests of normality and adjustment for multiple comparisons
☐	☒ A full description of the statistical parameters including central tendency (e.g. means) or other basic estimates (e.g. regression coefficient) AND variation (e.g. standard deviation) or associated estimates of uncertainty (e.g. confidence intervals)
☐	☒ For null hypothesis testing, the test statistic (e.g. *F*, *t*, *r*) with confidence intervals, effect sizes, degrees of freedom and *P* value noted *Give P values as exact values whenever suitable.*
☒	☐ For Bayesian analysis, information on the choice of priors and Markov chain Monte Carlo settings
☒	☐ For hierarchical and complex designs, identification of the appropriate level for tests and full reporting of outcomes
☐	☒ Estimates of effect sizes (e.g. Cohen's *d*, Pearson's *r*), indicating how they were calculated

Our web collection on statistics for biologists contains articles on many of the points above.

Software and code

Policy information about availability of computer code

Data collection	Targeted amplicons sequencing data were collected and demultiplexed by an Illumina HiSeq XTen instrument. Whole mitochondrial genome sequencing data were collected and demultiplexed by an Illumina NovaSeq 6000 instrument. FACS gating data were collected on a FACSAria Fusion (BD Biosciences) using FACSDiva version 9.4 (BD Biosciences). The luminescence was detected by EnVision Multilabel Reader. The ABR signals were acquired, filtered, amplified using TDT System III (Tucker-Davis Technologies).
Data analysis	High-throughput sequencing data were analyzed by BE-Analyzer (http://www.rgenome.net/be-analyzer/#!) (Hwang G-H et al, BMC Bioinformatics, 2018) or CRISPResso2 (http://crispresso.pinellolab.partners.org/) (Clement, K. et al.Nat Biotechnol, 2019) for base editing (A·T-to-G·C, and C·G-to-T·A) and indels efficiencies. Mitochondrial genome-wide off-target sequencing data were aligned to the GRCh38 (release v102) reference genome using BWA (v.0.7.17), and BAM files were created with SAMtools (v.1.9) by fixing read pairing information and flags. And data were processed using the REDItoolDenovo.py script from REDItools (v.1.2.1). The ABR signals were analyzed using software (BioSig) manufactured by Tucker-Davis Technologies. FACS data was analyzed using FlowJo v.10. GraphPad Prism 9.3.1 was also used to analyze data.

For manuscripts utilizing custom algorithms or software that are central to the research but not yet described in published literature, software must be made available to editors and reviewers. We strongly encourage code deposition in a community repository (e.g. GitHub). See the Nature Portfolio guidelines for submitting code & software for further information.

Data

Policy information about availability of data

All manuscripts must include a data availability statement. This statement should provide the following information, where applicable:

- Accession codes, unique identifiers, or web links for publicly available datasets
- A description of any restrictions on data availability
- For clinical datasets or third party data, please ensure that the statement adheres to our policy

Targeted amplicon sequencing data have been deposited in the NCBI Sequence Read Archive database under Accession Code PRJNA1249660, PRJNA1249952 and PRJNA1249944. Whole mitochondrial genome sequencing data have been deposited in the NCBI Sequence Read Archive database under accession codes under PRJNA1249252.
Cryo-electron microscopy structure of TadA-8e in complex with the DNA substrate was obtained from Protein Data Bank (PDB) under Accession Code 6VPC.
Plasmids are available on Addgene.

Research involving human participants, their data, or biological material

Policy information about studies with human participants or human data. See also policy information about sex, gender (identity/presentation), and sexual orientation and race, ethnicity and racism.

Reporting on sex and gender	N/A
Reporting on race, ethnicity, or other socially relevant groupings	N/A
Population characteristics	N/A
Recruitment	N/A
Ethics oversight	N/A

Note that full information on the approval of the study protocol must also be provided in the manuscript.

Field-specific reporting

Please select the one below that is the best fit for your research. If you are not sure, read the appropriate sections before making your selection.

☒ Life sciences ☐ Behavioural & social sciences ☐ Ecological, evolutionary & environmental sciences

For a reference copy of the document with all sections, see nature.com/documents/nr-reporting-summary-flat.pdf

Life sciences study design

All studies must disclose on these points even when the disclosure is negative.

Sample size	Experiments were performed in biological triplicate n=3 unless otherwise noted. Sample sizes were opted to display the range and consistency of differences and three biological replicates made it sufficient to support the conclusions in this research. Sample sizes for these experiments were chosen based upon fields standards and prior knowledge of experimental variation.
Data exclusions	No data were excluded from the analysis.
Replication	Three independent biological replicates were performed on different days. All replications were successful.
Randomization	Samples were randomly distributed into groups.
Blinding	Investigators were not blinded to group allocation in this research since experimental conditions were evident and all samples of treatment were consistent throughout experiments.

Reporting for specific materials, systems and methods

We require information from authors about some types of materials, experimental systems and methods used in many studies. Here, indicate whether each material, system or method listed is relevant to your study. If you are not sure if a list item applies to your research, read the appropriate section before selecting a response.

Materials & experimental systems

n/a	Involved in the study
☒	☐ Antibodies
☐	☒ Eukaryotic cell lines
☒	☐ Palaeontology and archaeology
☐	☒ Animals and other organisms
☒	☐ Clinical data
☒	☐ Dual use research of concern
☒	☐ Plants

Methods

n/a	Involved in the study
☒	☐ ChIP-seq
☐	☒ Flow cytometry
☒	☐ MRI-based neuroimaging

Eukaryotic cell lines

Policy information about cell lines and Sex and Gender in Research

Cell line source(s)	Human HEK293T cells (ATCC, CRL-3216), and PC12 cells (ATCC, CRL-1721).
Authentication	Human HEK293T Cells were authenticated by the supplier using STR analysis. PC12 cells were detected by small irregularly shaped cells and 40 chromosomes. Mitochondrial COI gene sequencing can confirm Rattus norvegicus origin.
Mycoplasma contamination	All cell lines used were tested negative for mycoplasma contamination.
Commonly misidentified lines (See ICLAC register)	No commonly misidentified cell lines were used.

Animals and other research organisms

Policy information about studies involving animals; ARRIVE guidelines recommended for reporting animal research, and Sex and Gender in Research

Laboratory animals	Sprague-Dawley strain rats used in this study were purchased from Shanghai Jihui Textile Technology Co., Ltd. Rats were maintained in specific pathogen-free facilities at 20-22 °C with 40-60% humidity under a 12 h light-dark cycle. 4-6 week-old female wild-type SD rats and 6-12 week-old female wild-type SD rats were used as embryo donors and foster mothers, respectively.
Wild animals	No studies with wild animals were performed.
Reporting on sex	To minimize variability and facilitate randomisation, femals and females were all used in this paper.
Field-collected samples	No studies with field-collected samples were performed.
Ethics oversight	All animal experiments met the regulations drafted by the Association for Assessment and Accreditation of Laboratory Animal Care in Shanghai and were approved by the Experimental Animal Welfare Ethics Committee of East China Normal University.

Note that full information on the approval of the study protocol must also be provided in the manuscript.

Plants

Seed stocks	N/A
Novel plant genotypes	N/A
Authentication	N/A

Flow Cytometry

Plots

Confirm that:

☒ The axis labels state the marker and fluorochrome used (e.g. CD4-FITC).

☒ The axis scales are clearly visible. Include numbers along axes only for bottom left plot of group (a 'group' is an analysis of identical markers).

☒ All plots are contour plots with outliers or pseudocolor plots.

☒ A numerical value for number of cells or percentage (with statistics) is provided.

Methodology

Sample preparation	Cell culture and transfection procedures are described in the methods. Cells were washed and filtered through a 45µm cell strainer cap before sorting (72h after transfection).
Instrument	FACSAria Fusion (BD Biosciences)
Software	FACSDiva version 9.4
Cell population abundance	The number of HEK293T cell and PC12 cells gated for target populations were similar in different biology replicates.
Gating strategy	For HEK293T cells and PC12 cells, gates were drawn to collect subsets of EGFP- and mCherry-double positive cells. Detailed gating strategy is provided in the Supplementary Note.

☒ Tick this box to confirm that a figure exemplifying the gating strategy is provided in the Supplementary Information.